Preparation and Characterization of Reduced Graphene Oxide/Titanium Dioxide Composites by Hydrothermal Method

G. Santamaría-Juárez, E. Gómez-Barojas, E. Quiroga-González, E. Sánchez-Mora, and J. D. Santamaría-Juárez

Abstract—In the present work, reduced graphene oxide/Titanium dioxide (rGO/TiO_2) composites (1:1 and 1:2 "in weight" (in wt) have been synthesized by the hydrothermal method using graphene oxide (GO) and commercial TiO_2 as precursors. Previously, we prepared the GO, in the way optimizing and making safer, the Hummers route. We have chosen the hydrothermal method to prepare the composites because it offers several advantages: 1) It consist of a very simple experimental setup, 2) it utilizes only water, instead of Hydrazine or Sulfonate used as chemical reductants in traditional methods, avoiding the incorporation of un-willing impurities into GO sheets, 3) the temperature and pressure condition reached in the closed hydrothermal system have promoted the recovery of π-conjugation after dehydration diminishing defects concentration and increasing the degree of reduction of the GO sheets, and 4) this system is compatible with industrial batch production. The structure, surface morphology, chemical composition and optical properties of GO, TiO_2 and rGO/TiO_2 composites have been analyzed using, TEM, FTIR, Raman- and XPS-spectroscopy. TEM micrographs show that the TiO_2 nanoparticles are non-homogenously adsorbed onto the GO sheets. FTIR spectra of the rGO/TiO_2 composites suggest that during the hydrothermal process the GO sheets get reduced. Raman spectra suggest that TiO_2 remains with anatase structure even after the hydrothermal process. The C 1s XPS spectra of the rGO/TiO_2 composites have shown a significant decrease of oxygenated carbon related signals, confirming that most of the oxygenated groups were successfully removed. Based on these characterization results we infer that, GO sheets of good quality have been successfully synthesized and the GO sheets have been partially reduced via the TiO_2 nanoparticles anchored during the hydrothermal process.

***Index Terms*— Graphene Oxide; TiO_2; Raman; XPS.**

I. INTRODUCTION

The research and development of new materials with better photocatalytic properties have drawn increasing attention driven by the motivations of exploring new materials with better photocatalytic properties. The TiO_2 is a semiconductor with a direct energy bandgap (3.2 eV) in the UV range of the electromagnetic spectrum [1]. The TiO_2 is the material most commonly used as a photocatalyst due to chemical and thermal stability, high efficiency and low cost, etc [2-6]. The TiO_2 exists in nature in two tetragonal forms, rutile and anatasa structures, and in a rhombic form called brookita. However, the anatasa structures seems to be more active photocatalytically probably due to differences in the extent and nature of the surface hydroxyl groups [2]. This semiconductor TiO_2 is synthesized by the hydrolysis of the $TiCl_4$ in a hot flame. This technique produces TiO_2 of about 4:1 anatase to rutile crystal structures ratio with specific surface area (~50 m^2/g) [3,4].

The photochemical application of TiO_2 photocatalysis is invariably affected by the surface properties of the TiO_2 particle and the photoinduced effect is affected by quantum size [5]. In photocatalisys application, commercial TiO_2 Degussa P25, is commonly used for example in: hydrogen production [6,7], water purification [8,9], and air detoxification [10,11].

In the past few decades, in order to increase the efficiency of the redox reaction involved in the photocatalysis process, the TiO_2 particles has been anchoring onto large-surface-area materials such as mesoporous, zeolites and low dimensional carbon-based materials [5,12-14].

In this context graphene, one-atom-thick planar sheet of carbon atoms densely packed in a honeycomb crystal lattice, has emerged as a high potential material due to its high surface area (theoretical value 2630 m^2/g) [15], mechanical flexibility, optical transparency, electrical conductivity [16] and good interface contact with adsorbents among other properties. The structure and properties of graphene depend on the synthesis method. Up today, several techniques have been established for graphene synthesis but mechanical cleaving (exfoliation) [17], chemical exfoliation [18], chemical synthesis [19], and thermal chemical vapor deposition (CVD) [20] are the most commonly used methods.

Nowadays, the only route that affords graphene-based sheets in considerable quantities relies on the chemical conversion of graphite to graphite oxide. Graphite oxide often called graphitic acid or graphitic oxide is a polycyclic aromatic hydrocarbon oxide interrupted by epoxides, alcohols, ketone carbonyls, and carboxylic groups [20-23].

Brodie et al. [24] first demonstrated the synthesis of graphite oxide in 1859 by adding a portion of potassium chlorate ($KClO_3$) to slurry of graphite in the presence of fuming nitric acid. It was until 1898 that Staudenmaier improved Brodie's method by replacing about two thirds of

Published on September 24, 2019.

G. Santamaría-Juárez and E. Gómez-Barojas are with CIDS-IC, Benemérita Universidad Autónoma de Puebla (BUAP). PO Box 196, Puebla, Pue., 72000, México.

E. Quiroga-González and E. Sánchez-Mora are with the Institute of Physics, BUAP. PO Box J-48, Puebla, Pue.,72570, México.

J. D. Santamaría-Juárez is with the Faculty of Chemical Engineering, BUAP. PO Box J33, Puebla, Pue., 72570, México.

Correspondence author. E-mail: egomez@ifuap.buap.mx, equiroga@ieee.org.

fuming HNO_3 by concentrated H_2SO_4 increasing the acidity in the mixture besides he added $KClO_3$ as the oxidant agent in nitric acid, minimizing in this way the risk of explosion [25]. However, in 1958 Hummers and Offeman [26] developed a method for the synthesis of graphite oxide based in all former developments but with key improvements. It consists of carrying out a reaction of graphite powder with $KMnO_4$ and $NaNO_3$ as oxidant agents in concentrated H_2SO_4. Since then, this method has been the most important and widely used for the synthesis of graphite oxide. Additionally, the graphite oxide can be exfoliated in many polar solvents and dispersed particularly well in water obtaining graphene oxide (GO) nanosheets.1q` 1

Since the graphene based composites can be processed from aqueous and polar solvents, they offer the convenience to cast thin films for various technological advances. For example, the anchoring of catalyst particles on carbon nanostructures can provide new ways to increase the surface area and improve: the catalysis performance of energy conversion devices, the enhanced electrocatalytic activity of semiconductor particles dispersed on carbon sheets of fuel cells [27,28], TiO_2/carbon nanotube composites have been established as viable potential photocatalysts for use in both water and air purifications [9,29]. The synergetic effect of carbon nanotubes on photocatalyst enhancement, in which carbon nanotubes act as the electron sink for the hindrance of charge carrier recombination [9] or as the photosensitizer to generate a greater concentration of electron/hole pairs [29] has been previously demonstrated. Carbon nanotubes (CNT) also behave as impurities, resulting in the formation of Ti–O–C bonds and, therefore, expanding the light absorption to longer wavelengths [30]. For this reason, the two dimensional carbon nanostructures such as graphene can also potentially serve as a support material on which semiconductor particles can be anchored to improve the performance of optoelectronic and energy conversion devices.

The aim of this research work is to incorporate oxygen containing groups on carbonaceous sheets via oxidation with strong acids to form a stable GO suspension in water and anchor TiO_2 particles on the GO sheets by means of a hydrothermal method to form rGO/TiO_2 composites with different TiO_2 concentrations. Microscopy and spectroscopy techniques are used to analyze the oxidation-reduction degree of the composites.

II. Experimental Part

A. Synthesis of GO4

GO was synthesized by carrying out the oxidation process of graphite powder in accord to the "safer modified Hummers' method" [31]. We started the synthesis of graphite oxide by using graphite powder (Bay carbon, spectroscope powders, Bay *City, Michigan 48706, ~100 μm) and* added a mixture of graphite and $KMnO_4$ powders (3:18 g; 3:6 in wt) into an H_2SO_4/H_3PO_4 solution (360:40 ml; 9:1 v/v proportion). One of the sub-products of the $KMnO_4$ and H_2SO_4 reaction is Mn_2O_7 which detonates at temperatures above 55 °C [32] thus, to prevent an explosion we cooled down both mixtures before mixing them. Consequently, only a slightly exothermal reaction took place at 35-40 °C and the solution turned purple-brown color. Next, the mixture was heated at 50 °C with continuous stirring for 12 h, at this point, the mixture turned dark brown indicating that the graphite oxidation reaction already took place. During this thermal process the mixture undergoes remarkable changes: gases are given off from the interior of the substance, which swells up the system in a most singular manner separating the carbonaceous sheets and reducing them to the minutest state of division which have the appearance and the structure of lamellar graphite [24], larger surface areas of the carbonaceous sheets are in contact with the $KMnO_4$ increasing their oxidation state. Based on these experimental results we infer that 12 h of the oxidation process is the appropriate time in which an efficient graphite oxidation *reaction takes place.*

Continuing with the rinsing procedure, the mixture was let cool down to room temperature, afterwards 400 ml of DI water in ice form was added to decrease its viscosity and avoid overheating [33, 34]. Later on, 9 ml of H_2O_2 (H_2O_2/DI water, 30% v/v) was added to the mixture to make easier the removal of metal salts such as permanganate and manganese residuals from the mixture, now this solution turned to a bright yellow color. The solution was centrifuged at 1500 rpm for one hour and the supernatant decanted away. The remainder was repeatedly rinsed in continuous succession with: 1) 200 ml of DI water, 2) 200 ml of HCl at 30% v/v and 3) 200 ml of ethanol to remove the byproducts (e.g., potassium-containing compounds) that can cause an acute explosion [35]; after each rinsing step, the solution was centrifuged at 4000 rpm for 2 h and the supernatant decanted away. Then, the remainder obtained after the rinsing procedure was coagulated with 40 ml of ether. Later on, the resulting suspension was filtered through a PTFE membrane with 0.45 μm pore size. Finally, the solid material obtained on the filter was vacuum-dried for overnight at room temperature. To remove water from graphite oxide, we carried out a thermal treatment at 60 °C (temperature below the one of graphite oxide reduction) under nitrogen flux for 2 h. The final product in powder form weighted 6.8 g. By considering a graphite initial weight of 3 g, it is estimated that about 80 % of carbon is linked to oxygen in different ways, including $^{-}$OH groups.

Since it is already known that chemically both graphite oxide and GO have similar or identical structures; both possess stacked structures with chemical functionality on their basal planes and at their edges [32]. The only difference between them is the number of stacked layers; GO possesses a monolayer or just a few stacked layers, while graphite oxide contains a greater number of stacked layers [32]. Taking into account, that the formation of oxygenated functional groups in graphite oxide makes them easier to exfoliate it into monolayers of GO, we dispersed 1 mg of graphite oxide powder in 100 ml DI water by sonication for 10 min to obtain GO nanosheets. Then, the prepared samples were analyzed by microscopic and spectroscopic techniques.

B. Synthesis of rGO/TiO_2 Composites

The rGO/TiO_2 composites were prepared by means of a hydrothermal treatment. First, 0.05 g of graphite oxide was

added to 50 ml of DI water and the mixture was sonicated for 2 h to achieve a uniform dispersion of GO. Previously, commercial TiO_2 nanoparticles (P25 TiO_2, Degussa) were thermally treated at 550 °C for 2 h to obtain clean TiO_2 particles surface. Then, 0.05 g of TiO_2 was added slowly to the GO dispersion solution and further stirred for 1 h to ensure complete mixing. This mixture was transferred to a Teflon-lined autoclave and heated at 150 °C under static condition for 5 h then, the solution was let cool down to room temperature. Later on, it was centrifuged at 18000 rpm for 1 h and the supernatant was decanted away. This product was rinsed with DI water several times, centrifuged at 18000 rpm and dried in an oven at 60 °C for 6 h. The final product is the rGO/TiO_2 composite at 1:1 in wt. By the same procedure, but doubling the amount of TiO_2, it was obtained the rGO/TiO_2 composite 1:2 in wt.

III. Results And Discussion

A. Characterization Techniques

The surface morphology of the GO, TiO_2 and rGO/TiO_2 samples was analyzed using a high-resolution transmission electron microscope (HRTEM) JEOL JEM-2100F, operated at 200 kV acceleration voltage. FTIR spectra (400-2000 cm^{-1}) were collected with a Spectrum One Perkin Elmer system with an ATR accessory using a scan velocity of 8 nm/s. Raman spectra were recorded with a Scientific DXR, Thermo SCIENTIFIC Raman system with a He-Ne laser (λ = 632.8 nm) with 10 mW of power as excitation source. The entrance and exit slits aperture was 50 µm. An optical microscope is coupled to this system and 10X magnification was used to select the region of interest. An X-ray photoelectron spectroscopy (XPS) system K-Alpha+ Thermo Scientific, with a Constant Analyzer Energy (CAE) was used to give insights about the chemical nature of the surface of the composites. XPS gives quantitative information about chemical groups and the chemical shift in XPS is a measure of the valence charge on the atom of interest. XPS spectra were obtained by irradiating the samples with an Al K_α (1486.6 eV) X-ray beam in an analyzing chamber with pressure of $2x10^{-9}$ Torr.

B. Morphological characterization

The surface morphology of the synthesized GO, TiO_2 and rGO/TiO_2 composites was analyzed by means of TEM (see Figure 1(a)). It can be observed that the morphology of GO is sheet like. The sheets look translucent, well defined with some wrinkles on the surface and with no folding on the edges. In these micrographs it can be observed some imperfections, dark and light zones and some dark points on the surface that cause some irregularities on the plane surface. These imperfections are related with the existence of carbon atoms with sp^3 hybridization that constitute the hydroxyl or epoxy groups on the GO sheets [36]. In the inset of this figure it is shown an HRTEM image of the GO. Figure 1(b) shows TEM micrographs of TiO_2 (Degussa P25). It is observed that, as expected, the morphology of TiO_2 powder consists of agglomerations of particles of different shapes and sizes. In the inset of Figure 1(b), it is seen a cluster of particles with irregular shape and length of about 20 nm. Figure 1(c) shows TEM micrographs of the rGO/TiO_2 composite in proportion 1:1 in wt. It is observed that TiO_2 particles cover the whole GO surface. In Figure 1(d) a TEM micrograph of the rGO/TiO_2 composite 1:2 in wt is shown. Once again a conglomeration of TiO_2 particles is observed, this conglomeration causes a nonhomogeneous distribution of TiO_2 on the GO sheets. According to the insets in Figure 1(c,d), the size of the TiO_2 particles in both composites is about 40 nm due to the same conditions of temperature and pressure used in the hydrothermal process.

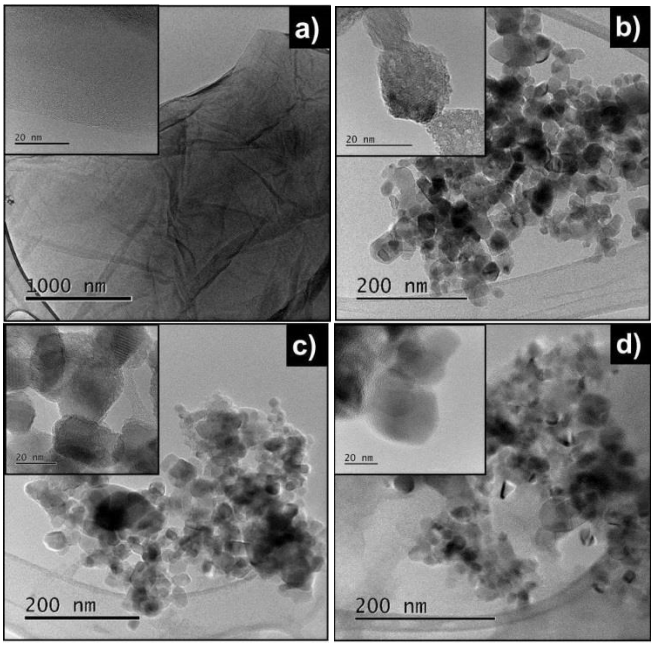

Fig. 1. TEM micrographs of: (a) GO, (b) TiO_2, and rGO/TiO_2 composites in proportion: (c) 1:1 and (d) 1:2 in wt and the corresponding insets of HRTEM images.

C. EDS

The standardless quantification of the Energy Dispersive Spectroscopy (EDS) spectra of the samples under analysis are: for GO: 83.9 wt % of carbon and 16.1 wt % of the Oxygen element. For the TiO_2 single compound is: Oxygen 55.3 wt % and Titanium 41.7 wt %. The one of the rGO/TiO_2 composite 1:1 in wt is: Titanium 42.1 wt %, Oxygen 16.1 wt % and Carbon 24.9 wt% and the one of the rGO/TiO_2 composite 1:2 in wt is: 55.3 wt % Carbon, 29.5 wt % Oxygen and 15.3 wt % of Ti.

Additional information about the elements concentrations can be observed in the EDS mapping images: Figure 2(a) shows a TEM image of the region of interest of the rGO/TiO_2 composite 1:1 in wt. EDS mapping images are shown: in (b) carbon in red, (c) oxygen in blue, (d) Titanium in green and e) the overlay of the three mappings. It is observed that the four elements are adsorbed in a common region of the GO sheets.

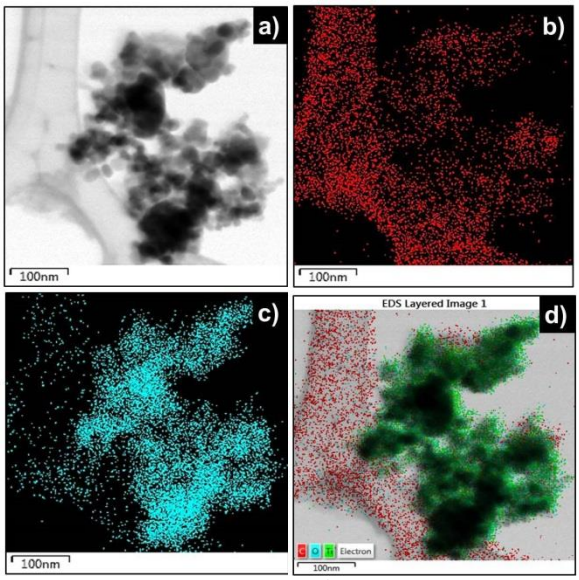

Fig. 2. Elemental Mapping images of the rGO/TiO_2 composite in proportion 1:1 in wt. In (a) the gray image of the region under analysis, in (b) Carbon in blue, (c) Oxygen in yellow and (e) the color overlay of the three mappings.

Finally, Figure 3 shows the elemental mapping images of the rGO/TiO_2 composite 1:2 in wt. In (a) the gray image of the region under analysis, in (b) Carbon in blue, (c) Oxygen in yellow, (d) Titanium in pink and (e) the color overlay of the three mappings. Thus, we can infer that the Ti atoms are non-homogeneously adsorbed on the GO sheets.

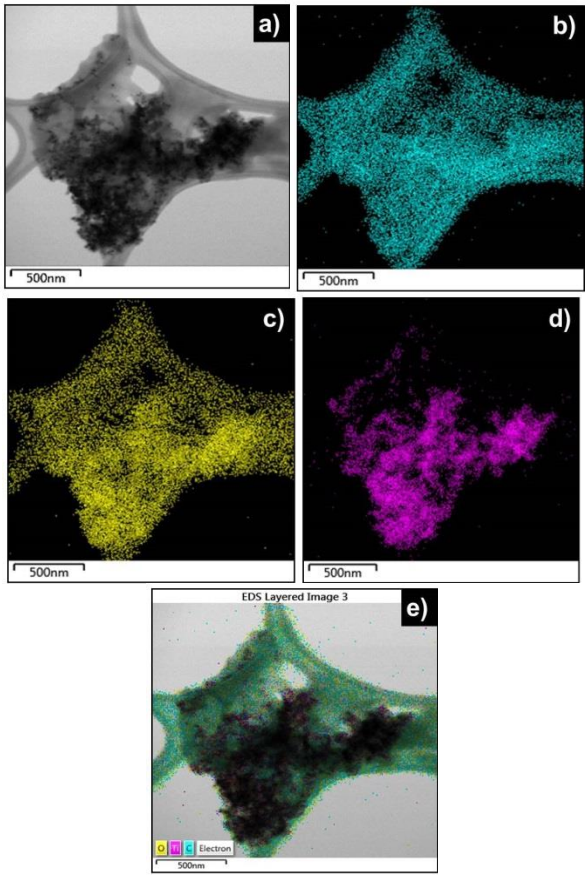

Fig. 3. Elemental Mapping images of the rGO/TiO_2 composite in proportion 1:2 in wt. In (a) the gray image of the region under analysis, in (b) Carbon in blue, (c) Oxygen in yellow, (d) Titanium in pink and (e) the color overlay of the three mappings.

D. FTIR spectroscopy

Figure 4(a) shows an FTIR transmission spectrum recorded from GO in the range from 4000 to 700 cm^{-1}. In this spectrum appear different peaks that are assigned to vibrational modes of oxygen-containing functional groups; for a better visualization see points (A), (B) and (C) on the inset of this figure. Additionally, C=C and C-O vibrations of GO are also present, as expected. It is worthy to mention that the FTIR spectrum of GO recorded after one year is very similar to the one recorded from the fresh GO, this means that GO is stable with respect to aging.

In Table 1 the measured peaks positions, the reported ones, and their assignments according to the literature are listed. There is a good concordance between the two groups. We infer then, that the GO nanosheets are covered by functional groups such as hydroxyl (-OH), epoxy (C-O-C) and carboxylic (-COOH) groups. It is worthwhile to mention that the FTIR spectrum of GO recorded after one year is very similar to the one recorded from fresh GO, this means that GO is stable with respect to aging.

TABLE I: GO VIBRATIONAL MODES ASSIGNMENTS REPORTED IN THE LITERATURE AND MEASURED.

Reported Peak Position (cm^{-1})	Measured Peak Position (cm^{-1})	Functional	Reported Peak Position (cm^{-1})	Measured Peak Position (cm^{-1})
3410	3407	Water (-OH)	stretching	[37]
1734	1734	Carboxylates or Ketone (C=O)	stretching	[38,39]
1734		Water (-OH)	bending	[39,40]
1629	1625	Bonding C=C	stretching	[41]
1420	Not found	Alcohols (C-OH)	bending	[40,41]
1227	1225	Epoxide (C-O-C) or Phenols (C-O-H)	stretching	[42,43]
1055	1055	Bonding C-O	stretching	[32,43]

In Figure 4(b) the FTIR transmission spectrum of TiO_2 is shown; the 3 peaks located at 3440 cm^{-1}, 1630 and 1430 cm^{-1} are associated to a tension vibrational mode of H-OH, to the flexion vibrational mode of water and to vibrational modes of residual C-H organic groups, respectively. These residual groups come from the reactants used during the synthesis process and to the TiO_2 nature [44]. On the other hand, in the range 800 - 400 cm^{-1} the bands of TiO_2 with anatasa structure are present: the one at 466 cm^{-1} associated with the Ti-O vibrational mode, and the bands close to 515 cm^{-1} and 715 cm^{-1}, assigned to vibrational modes of the Ti-O-Ti bonds [45].

In Figure 4(c) transmission FTIR spectra of rGO/TiO_2 1:1 in wt and rGO/TiO_2 1:2 in wt are shown. As mentioned before, these spectra suggest that during the solvothermal process the GO gets reduced, that is, the GO loses oxygenated groups and consequently the sp_2 Carbon bonds band increases in intensity becoming reduce graphene oxide (rGO) sheets. This effect is observed clearly in Figure 4(d) by the intensity increase of the band at 1600 cm^{-1}, corresponding to C=C bonds. Besides, TiO_2 binds to the GO surface by means of C-O bonds clearly seen by the presence of the band at 1734 cm^{-1} of the composites spectra.

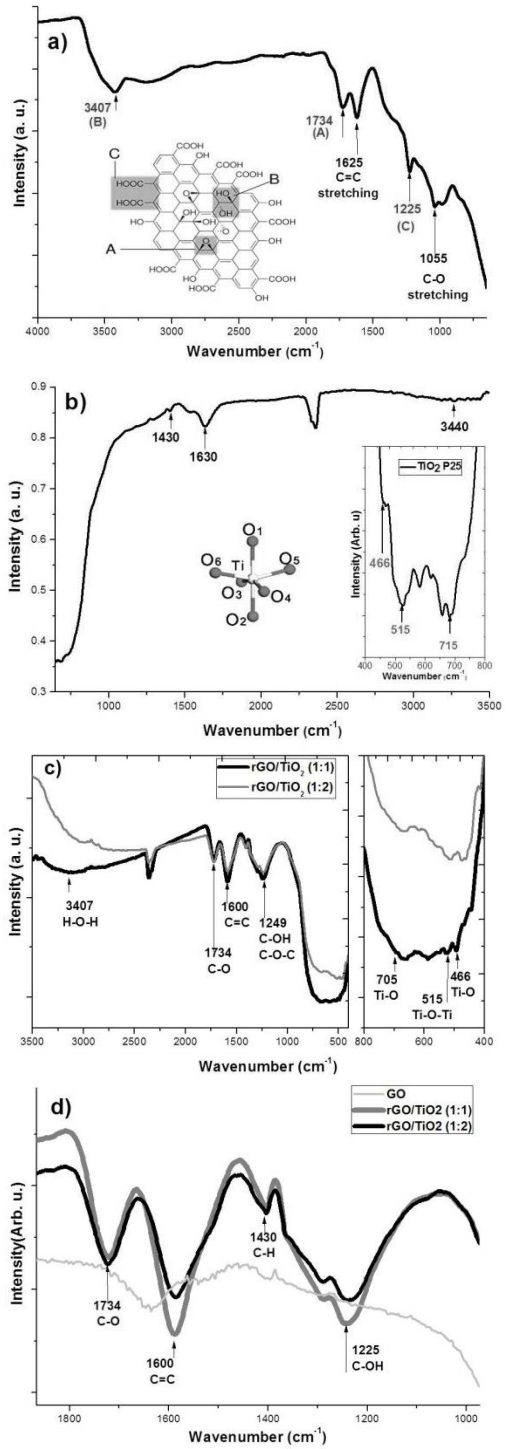

Fig. 4. FTIR spectra of: (a) GO, (b) TiO_2, (c) rGO/TiO_2 composites: 1:1 and 1:2 in wt and (d) FTIR spectra of the composites in a reduced range.

E. *UV-Vis spectroscopy*

We used the UV-Vis spectroscopy technique to monitor the reduction of GO. In Figure 5, normalized UV-Vis absorbance spectra (in the range: 200-800 nm) of GO, rGO/TiO_2 1:1 in wt and rGO/TiO_2 1:2 in wt composites are shown. In the GO spectrum it is observed an absorption band with maximum at 230 nm characteristic of GO due to transitions π-π^* in its graphitic structure (interactions of orbitals π in bonding C=C and π^* in bonding C-C) [46]. Also it is observed, on the adsorption edge a shoulder at 300 nm corresponding to oxygenated groups. On the other hand, the absorbance spectrum of the rGO/TiO_2 composite 1:1 in wt presents an absorption band with maximum at 264 nm, that is 34 nm red shifted with respect to 230 nm of the GO peak and in the spectrum of rGO/TiO_2 1:2 in wt the corresponding maximum appears at 254 nm, that is 24 nm red shifted with respect to the one of GO peak (see the inset in Figure 5, that shows the top parts of the bands). These red shifts are due to reduction of GO [47], suggesting that the GO in both composites might be reduced and the aromatic structure might be restored gradually. The reduction of the GO when forming the rGO/TiO_2 composites 1:1 and 1:2 in wt is probably due to superheated H_2O that promotes an acid-catalyzed reaction of organic compounds because it generates a sufficiently high H^+ concentration to remove oxygenated groups on the surface GO sheets. In other words, the GO reduction is indicative of the restoration of the π-conjugation network within the graphene nanosheets.

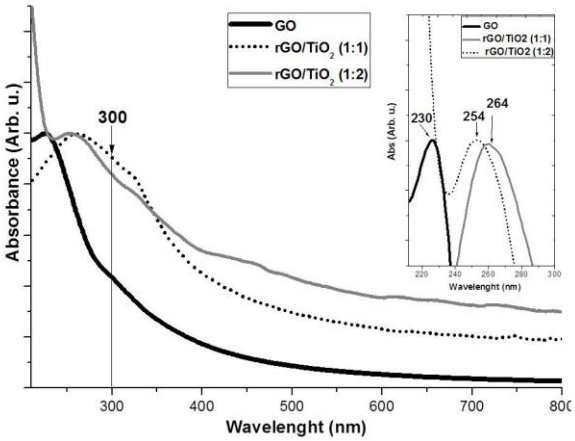

Fig. 5. UV-vis absorbance spectra of: GO, rGO/TiO_2 composites: 1:1 and 1:2 in wt.

These results obviously demonstrate the significant influence of graphene oxide on the optical characteristics in which increasing graphene oxide amount narrows the band gap of TiO_2. Similar to the case of TiO_2-CNT, C-doped TiO_2 or TiO_2- chemically converted graphene composites, the phenomena in this study could be ascribed to the formation of Ti–O–C chemical bonding in the prepared composites [48-51].

F. *Raman spectroscopy*

Raman spectroscopy is a valuable tool to characterize carbon based materials. Figure 6(a) shows the Raman spectrum of graphite oxide. It consists of a first order (1100-1800 cm^{-1}) and second order (2500–3100 cm^{-1}) regions [52,53]. In the former region appears the D band at 1350 cm^{-1} assigned to the presence of defects such as: bond-angle disorder, bond length disorder, vacancies, and edge defects and a G band at 1580 cm^{-1} that corresponds to the E_{2G} vibration mode of a crystal with D_{6h}^4 symmetry [36]. Also, in the second order scattering range appears at 2700 cm^{-1} the 2D band also called D+G band or G' band which is an overtone of the D band [36]. The Raman spectrum shown in Figure 6(a) is very similar to the one reported in the literature by Kuila, et al. [41] therefore, we infer that the processes we have performed to graphite powder in order to obtain GO are appropriate.

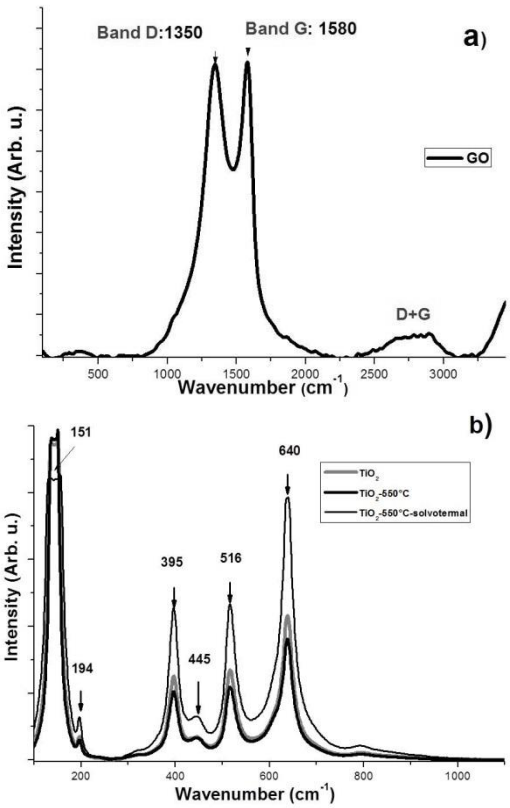

Fig. 6 Raman spectra of a) GO and b) TiO_2.

Furthermore, Figure 6(b) shows overlapped Raman spectra in the range 100-900 cm^{-1} corresponding to: as received TiO_2, TiO_2 thermally treated at 550 ˚C and to TiO_2 solvothermally treated at 550 ˚C. The Raman scattering bands appearing at 151, 194, 395, 516 and 640 cm^{-1} correspond to TiO_2 with anatase phase and the low intensity band at 445 cm^{-1} corresponds to the rutile phase [54] which means that a low contribution of the rutile phase is present in the TiO_2 anatase phase. As can be seen the three spectra are very similar except that the one of TiO_2 solvothermally treated is intensified.

Figure 7 shows overlapped Raman spectra (100-3500 cm^{-1}) of the rGO/TiO_2 composites: 1:1 and 1:2 in wt. In the range 100-650 cm^{-1} appear the Raman lines at 144, 396, 509 and 632 cm^{-1}. The peaks positions are slightly shifted with respect to the ones of TiO_2 as received. In the range 1100-1800 cm^{-1} appear the Raman lines corresponding to GO: the D band at 1347 cm^{-1} and the G band at 1593 cm^{-1} (see inset (a) in Figure 7). These bands are slightly shifted with respect to the GO single compound. However, we highlight the displacement of the G band from 1580 cm^{-1} to 1593 cm^{-1}; this shifting is attributed to the regeneration of double bonds on the carbonaceous sheets that resonate at higher frequencies [55-57] suggesting that the GO sheets in our composites have been partially reduced.

The intensity ratio (I_D/I_G) of D band to G band of the GO is about 0.96 indicating a minimum concentration of defects in the carbonaceous sheets. Hydrothermal treatment at 180 ˚C for 6 h decreased the I_D/I_G ratio to 0.90 (Figure 4(b)). This suggests that the hydrothermal reaction, besides dehydrating/reducing the GO is also able to recover the aromatic structures by repairing defects. Therefore, we could conclude that the hydrothermal reduction route is more effective in repairing the sp_2 network than the reduction process using other solvents [33]. An appropriate variation of the hydrothermal process temperature would allow us to control the extent of conversion of GO to graphene.

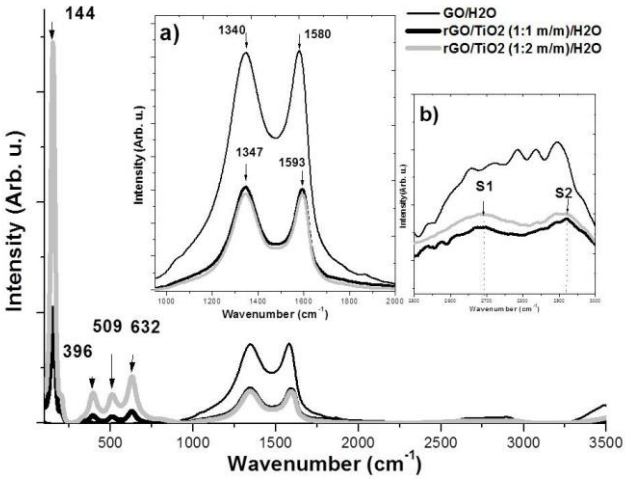

Fig. 7. Overlapped Raman spectra of the rGO/TiO_2 composites: 1:1 and 1:2 in wt.

The small S1 at 2701 cm^{-1} and S2 at 2900 cm^{-1} bands included in the 2D band (see inset (b) in Figure 7) suggest the presence of graphitic material of low crystallinity, the loss of functional groups and the consequent formation of C-H new bonds [58]. The TiO_2 nanoparticles could improve GO dispersion and the defects concentration could diminish by their restructuration.

G. XPS spectra

The chemical state of the GO, TiO_2 and the composites rGO/TiO_2 in 1:1 and 1:2 in wt were analyzed by the XPS technique. These spectra were excited with X rays AlK_α (1486.6 eV). Fig. 8a shows Oxygen XPS spectra, as a constituent element in: TiO_2, GO and in the composites rGO/TiO_2 in 1:1 and 1:2 in wt. Figure 8(b) shows the XPS spectra of Titanium as a constituting element in TiO_2, rGO/TiO_2 composites 1:1 and 1:2 in wt. Curve fitting was performed to all spectra using a Gaussian-Lorentzian peak shape after performing a Shirley background correction.

According to the XPS Wagner Handbook [59] the Ti 2p spectrum in the region 450-470 eV consists of the Ti $2p_{3/2}$ at 458.5 eV and Ti $2p_{1/2}$ at 468.2 eV binding energy. The energy difference between these two peaks is ΔE=5.66 eV. Figure 8(a) shows the XPS spectral peaks Ti 2p in TiO_2, rGO/TiO_2 composite 1:1 in wt and rGO/TiO_2 composite 1:2 in wt. The XPS spectral peaks in TiO_2 for the Ti $2p_{3/2}$ and Ti $2p_{1/2}$ are located at 458.72 and 464.38 eV respectively. The energy difference between these two peaks is ΔE=5.66 eV. The XPS spectral peaks in the rGO/TiO_2 composite 1:1 in wt for Ti $2p_{3/2}$ and Ti $2p_{1/2}$ are located at 459.8 and 465.5 eV respectively, the energy difference between these two peaks is ΔE=5.7 eV and the XPS spectral peaks in the rGO/TiO_2 composite 1:2 wt% for Ti $2p_{3/2}$ and Ti $2p_{1/2}$ are located at 459.00 and 464.72 eV respectively, the energy difference between these two peaks is ΔE=5.72 eV. According to these data we conclude that both composites contain TiO_2 and the Ti 2p position remains constant when the concentration of TiO_2 is varied to form the composites.

In order to observe the Ti-O bond evolution in the

composites, in Figure 8(a) overlapped O 1s XPS spectra of the: TiO_2, rGO/TiO_2 in 1:1 in wt, rGO/TiO_2 1:2 in wt and GO are shown. The maximum of the O 1s XPS spectrum is at: 530.06 eV that corresponds to Ti-O binding energy in TiO_2 single compound; it is at 533.17 eV for GO that could correspond to the presence of C-O-C, C-O-OH or C-OH groups at the surfaces of the carbon sheets [33]. While the maximum of the O 1s XPS spectrum is at 530.99 eV for the rGO/TiO_2 in 1:1 in wt corresponding to Ti-O binding energy and this maximum shifts to 530.20 eV for the Ti-O binding energy in the rGO/TiO_2 composite 1:2 in wt. It is observed clearly in Figure 8(a) that the Ti-O bond is shifted toward greater energies (530.90 eV) when Ti-O-C bonds are generated, while the Ti-O bond in the composite bearing oxides shifts to the Ti-O bonding energy in TiO_2 when the amount of this compound is increased in the composite, screening the Ti-O-C bond.

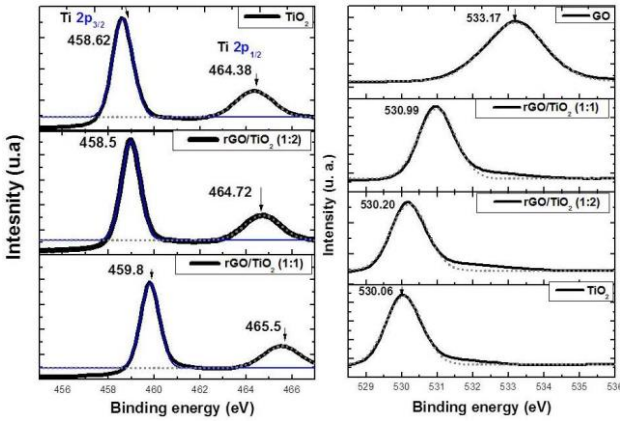

Fig. 8. XPS spectra of: a) Ti 2p in TiO_2 and in the composites: rGO/TiO_2 in 1:1 in wt and rGO/TiO_2 1:2 in wt and (b) O1s in GO, rGO/TiO_2 composite 1:1 in wt, rGO/TiO_2 composite 1:2 in wt and in TiO_2.

Fig. 9 shows XPS spectra of C 1s as a constituting element of: a) GO, b) rGO/TiO_2 composite 1:1 in wt and c) rGO/TiO_2 composite 1:2 in wt. The C 1s in the XPS spectrum of GO shows 3 components: at 284.6 eV (FWHM=1.4 eV), 286.5 eV (FWHM=1.2 eV) and at 287.6 eV (FWHM= 2.0 eV). These peaks correspond to: non-oxygenated rings (284.6 eV), that include C-C, C=C, and C-H bonds; the C-O bond in the C-O-C or C-OH group (286.5 eV); and C=O bond (287.6 eV). The presence of these groups suggests a considerable degree of oxidation of the GO nanosheets [33].

High-resolution X-ray photoemission C 1s spectra of the composites show a significant decrease of oxygenated carbon related signals in the range 286-289 eV after hydrothermal process (Figure 9 (b,c)) confirming that most of the epoxide, hydroxyl, and carboxyl functional groups were successfully removed. XPS spectra of the hydrothermally treated sample show that this method does not incorporate impurities, and the only elements present are oxygen and carbon.

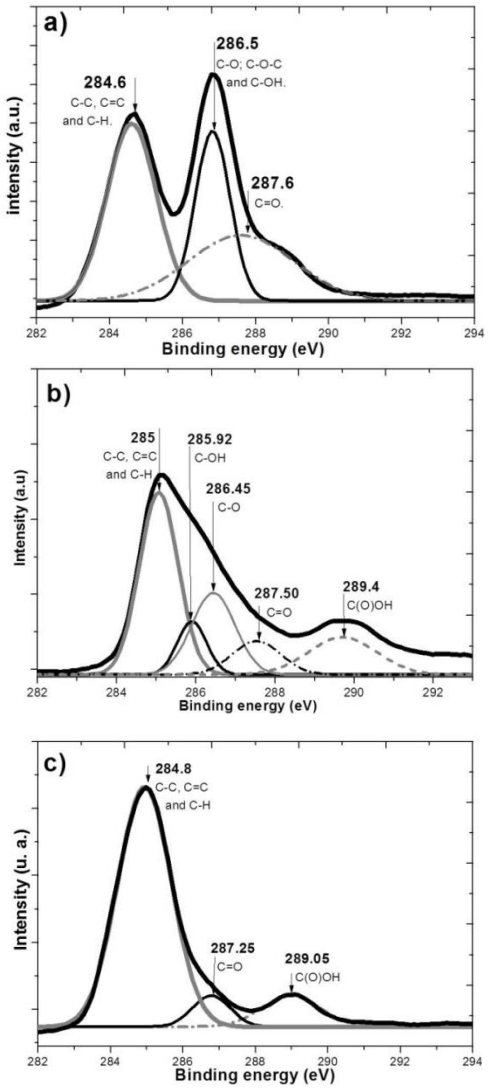

Fig. 9. XPS spectra of C 1s in: (a) GO, (b) rGO/TiO_2 composite 1:1 in wt and (c) in the rGO/TiO_2 composite 1:2 in wt.

The hydrothermal conversion method to reduce GO with TiO_2 has several advantages over the common chemical reduction processes, such as, 1) it requires very simple experimental setup, that is, basically an autoclave; 2) it has good upward scalability and it is industrially compatible with batch processing; 3) it is intrinsically pure because it utilizes only water instead of Hydrazine or Sulfonate to reduce GO, which unavoidably introduces noncarbon impurities into the treated GO [60]; 4) the closed system of relative high temperature and internal pressure promotes the recovery of π-conjugation after dehydration, which is favorable for minimizing defects [61]; and 5) engineering the parameters of temperature and pressure allows to control the degree of reduction of GO.

IV. Conclusion

We have synthesized GO following a safer and optimized modified Hummers' method [31]. We prepared the rGO/TiO_2 1:1 in wt and rGO/TiO_2 1:2 in wt using the hydrothermal method. HRTEM images of TiO_2 powder show particles of about 20 nm forming agglomerations. Similar TiO_2 clusters are observed in the composites but the size of the TiO_2 particles is increased to about 40 nm, that is,

the particles coalescence during the hydrothermal process. When the proportion of TiO_2 is increased to form the rGO/TiO_2 1:2 in wt composite the conglomerations get larger causing a nonhomogeneous distribution of the adsorbed TiO_2 on the GO sheets. FTIR spectra of the rGO/TiO_2 1:1 and 1:2 in wt suggest that during the solvothermal process the GO get reduced, that is, the GO loses oxygenated groups and consequently the sp_2 Carbon bonds are increased. This effect is indicated by the intensity increment of the band at 1600 cm^{-1} corresponding to C=C bonds. Also we could infer that TiO_2 binds the GO surface by means of C-O bonds as suggested by the appearance of the band at 1734 cm^{-1} of both spectra. According to the Raman spectra we conclude that the TiO_2 in the rGO/TiO_2 composites is in anatase phase. The Raman spectrum of GO shows the D and G bands typical of carbonaceous materials, and the corresponding bands appeared in the Raman spectra of the rGO/TiO_2 composites except that they are slightly shifted to lower energies, suggesting that the GO sheets in our composites have been partially reduced.

According to the XPS spectra of TiO_2 and the composites, we conclude that both composites contain TiO_2 and that the Ti 2p energetic position remains constant when the concentration of TiO_2 is doubled. The Ti-O bond is shifted toward greater energies (530.90 eV) when Ti-O-C bonds are generated, while the Ti-O bond in the composite bearing oxides shifts to the Ti-O binding energy in TiO_2 when the amount of this compound is increased in the composite screening the Ti-O-C bond. The XPS analysis allowed us to find out the chemical state of the GO sheets. High-resolution X-ray photoemission C 1s spectra (XPS) of the composites show a significant decrease of oxygenated carbon related signals at 286-289 eV after hydrothermal process, confirming that most of the epoxide, hydroxyl, and carboxyl functional groups were successfully removed. XPS spectrum of the hydrothermally treated sample shows that it has no impurities, and the only elements present are oxygen and carbon.

The main conclusion of this work is that GO sheets of good quality have been obtained, TiO_2 particles were anchored to the GO sheets by means of a hydrothermal process and the GO sheets have turned out partially reduced.

ACKNOWLEDGMENT

This work has been partially supported by CONACYT through a post graduate student scholarship and by SEP-IFUAP- “Low Dimensional Structures” research group (CA-315).

REFERENCES

[1] P. Magalhães, L. Andrade, O. C. Nunes and A. Mendes. “Titanium dioxide photocatalysis: fundamentals and application on photoinactivation”, *J. Rev.Adv. Mater. Sci.* vol. 51, pp.91-129, 2017.

[2] Zhang, Jinfeng, Zhou, Peng, Liu, Jianjun, Yu, Jiaguo. “New understanding of the difference of photocatalytic activity among anatase, rutile and brookite TiO_2”, *J. Physical Chemistry Chemical Physics*, vol.16, pp. 20382- 20386, 2014.

[3] T. Cao, Y. Li, C. Wang, C. Shao, and Y. Liu. “One-step nonaqueous synthesis of pure Phase TiO_2 nanocrystals from $TiCl_4$ in butanol and their photocatalytic properties”. *J. of Nanomaterials*, vol. 2011, pp. 6, 2011.

[4] X. Chen and C. Burda. “The electronic origin of the visible-light absorption properties of C-, N- and S-Doped TiO_2 nanomaterials”. *J. Am. Chem. Soc*. vol. 130, pp. 5018–5019, 2008.

[5] U. Ibrahim, G. Abdul, H. Abdullah. “Heterogeneous photocatalytic degradation of organic contaminants over titanium dioxide: A review of fundamentals, progress and problems”. *J. of Photochemistry and Photobiology C: Photochemistry Reviews*, vol. 9, pp. 1-12, 2008.

[6] U. M. Khan, A. S. Mofareh, W. B. Ingler. “Efficient photochemical water splitting by a chemically modified n-TiO_2”, *J. Science*. vol. 297, pp. 2243–2245, 2002.

[7] X. B. Chen, S. H. Shen, L. J. Guo, S. S. Mao, “Semiconductor-based photocatalytic hydrogen generation”, *J. Chem. Rev.* vol. 110, pp. 6503–6570, 2010.

[8] A. Wold, “Photocatalytic properties of TiO_2”, *J. Chem. Mater*. vol. 5, pp. 280–283, 1993,

[9] M. R. Hoffmann, W. Choi, D. W. Bahnemann, “Environmental applications of semiconductor photocatalysis”, *J. Chem. Rev*. vol. 95 pp. 69–96, 1995.

[10] D.A. Trubitsyn, A.V. Vorontsov, Experimental study of dimethyl methylphosphonate decomposition over anatase TiO_2, *J. Phys. Chem. B*, vol. 109 pp. 21884–21892, 2005.

[11] T. Noguchi, A. Fujishima, P. Sawunyama, K. Hashimoto, “Photocatalytic degradation of gaseous formaldehyde using TiO_2 film”, *J. Environ. Sci. Technol*. vol. 32 pp. 3831–3833, 1998.

[12] S. Banerjee, S. K. Mohapatra, P. P. Das and M. Misra. “Synthesis of Coupled Semiconductor by Filling 1D TiO_2 Nanotubes with CdS”, *J. Chem. Mater*., vol. 20, pp. 6784-6791, 2008.

[13] C. Martín, M. Ziółek, M. Marchena, and A. Douhal. “Interfacial Electron Transfer Dynamics in a Solar Cell Organic Dye Anchored to Semiconductor Particle and Aluminum-Doped Mesoporous Materials”, *J. Phys. Chem. C*., vol. 115, 46, pp. 23183–23191, 2011.

[14] S. Agarwala, M. Kevin, A. S. W. Wong, C. K. N. Peh, V. Thavasi§ and G. W. Ho. “Mesophase ordering of TiO_2 film with high surface area and strong light harvesting for dye-sensitized solar cell”, *J. CS Appl. Mater. Interfaces*, vol. 2, pp. 1844–1850, 2010.

[15] A. Peigney, C. Laurent, E. Flahaut, R.R. Bacsa, A. Rousset. “Specific surface area of carbon nanotubess and brundles of carbon nanotubes”, *J. Carbon*, vol. 39, pp. 507-514, 2001.

[16] D. P. HansoraN. G. ShimpiS. Mishra. “Graphite to Graphene via Graphene Oxide: An Overview on Synthesis, Properties, and Application”. *The Minerals, Metals & Materials Society JOM*., vol. 67, pp. 2855-2868, 2015.

[17] K. S. Novoselov, D. Jiang, F. Schedin, T. J. Booth, V. V. Khotkevich, S. V. Morozov, and A. K. Geim. “Two-dimensional atomic crystals”. *Proceedings of the National Academy of Sciences*, vol. 102, pp. 10451-10453, 2005.

[18] Lisa M. Viculis, Julia J. Mack, Richard B. Kaner. “A Chemical Route to Carbon Nanoscrolls”, *J. Science*., vol. 299, pp. 1361, 2003.

[19] S. Park & R. S. Ruoff. “Chemical methods for the production of graphenes”, *J. Nature Nanotechnology*., vol. 4, pp. 217–224, 2009.

[20] A. Reina, S. Thiele, X. Jia, S. Bhaviripudi, M. S. Dresselhaus, J. A. Schaefer, J. Kong. “Growth of large-area single- and Bi-layer graphene by controlled carbon precipitation on polycrystalline Ni surfaces”, *J. Nano Res*. vol. 2, pp. 509 516, 2009.

[21] A. B. Bourlinos, D. Gournis, D. Petridis, T. Szabó, A. Szeri, I. Dékány. “Graphite Oxide: Chemical Reduction to Graphite and Surface Modification with Primary Aliphatic Amines and Amino Acids”, *J. Langmui*, vol. 19, pp. 6050–6055, 2003.

[22] S. Niyogi, E. Bekyarova, M. E. Itkis, J. L. McWilliams, M. A. Hamon, R. C. Haddon. “Solution Properties of Graphite and Graphene”, *J. Am. Chem. Soc.* vol. 128, pp. 7720–7721, 2006.

[23] W. Chen, L. Yan, and P. R. Bangal. “Chemical Reduction of Graphene Oxide to Graphene by Sulfur-Containing Compounds”, *J. Phys. Chem. C*, vol. 114, pp. 19885–19890, 2010.

[24] B C. Brodie. “On the atomic weight of graphite”, *Philos. Trans. R. Soc. London*, vol. 149, pp. 249–259, 1859.

[25] L.Staudenmaier. “Verfahren zur darstellung der graphitsäur”, *J. Ber. Dtsch. Chem. Ges*., vol. 31, 1481–1487, 1898.

[26] W. S. Hummers, R. E. Offeman. “Preparation of graphitic oxide”, *J. Am Chem Soc*., vol. 80, pp. 1339-1339, 1958.

[27] G. Girishkumar, T. D. Hall, K. Vinodgopal, P. V. Kamat. “Single Wall Carbon Nanotube Supports for Portable Direct Methanol Fuel Cells”. *J. Phys. Chem. B*., vol. 110, pp. 107–114, 2006.

[28] A. Kongkanand, S. Kuwabata, G. Girishkumar, P. Kamat. “Single-Wall Carbon Nanotubes Supported Platinum Nanoparticles with Improved Electrocatalytic Activity of Oxygen Reduction”, *J. Langmuir*, vol. 21, pp. 2392–2396, 2006.

[29] W.D. Wang, P. Serp, P. Kalck, J.L. Faria. “Visible light photodegradation of phenol on MWNT–TiO_2 composite catalysts

prepared by a modified sol–gel method", *J. Mol. Catal. A: Chem*., vol. 235, pp. 194–199, 2005.
[30] G. Pyrgiotakis, S.H. Lee, W.M. "Sigmund, Advanced Photocatalysis with Anatase Nano-coatedMulti-Walled Carbon Nanotubes", *M.R.S. Spring Meeting*, San Francisco, CA, 2005.
[31] Under review for publication.
[32] D. R. Dreyer, S. Park, Bielawski CW, R. S. Ruoff. "The chemistry of graphene oxide", *J. Chem. Soc. Rev*. vol. 39, pp. 228–240, 2010.
[33] P. Wang, J. Wang, T. Ming, X. Wang, H. Yu, J. Yu, Y. Wang, and M. Lei. "Dye-Sensitization-Induced Visible-Light Reduction of Graphene Oxide for the Enhanced TiO_2 Photocatalytic Performance", *ACS. J. Applied Materials & Interfaces*, vol. 5, pp. 2924-2929, 2013.
[34] G. Williams, B. Seger and P. V. Kamat. "TiO^2-Graphene Nanocomposites. UV-Assisted Photocatalytic Reduction of Graphene Oxide", *ACS. J. Nano*., vol. 2, pp. 1487–1491, 2008.
[35] N. E. Sorokina, M. A. Khaskov, V. V. Avdeev, I. V. Nikol'skaya. "Reaction of Graphite with Sulfuric Acid in the Presence of $KMnO_4$", *Russ J Gen Chem.* 75, vol. 2, pp. 162–8, 2005.
[36] K. Krishnamoorthy, M. Veerapandian and K. Yun. "The chemical and structural analysis of graphene oxide with different degrees of oxidation", *J. Carbon*. vol. 53, pp. 38- 49, 2013.
[37] T. M. Paronyan. "Incommensurate graphene foam as a high capacity lithium intercalation anode", *J. Sci. Rep*., vol. 7, pp. 39944, 2017.
[38] J. Shen, T. Li, Y. Long, M. Shi, N. Li, M. Ye. "One-step solid state preparation of reduced graphene oxide", *J. Carbon*, vol. 50, pp. 2134-2140, 2012.
[39] Q. Li, B. Guo, J. Yu, J. Ran, B. Zhang, H. Yan, J. Gong. J. Am. "Highly efficient visible-light-driven photocatalytic hydrogen production of CdS-cluster-decorated graphene nanosheets", *J Chem. Soc*. vol. 133, pp. 10878, 2011.
[40] M. Zhang, B. Qu, D. Lei, Y. Chen, X. Yu, L. Chen, Q. Li, Y. Wang, T. J. Wang. "A green and fast strategy for the scalable synthesis of Fe_2O_3/graphene with significantly enhanced Li-ion storage properties", *J Mater. Chem.* vol. 22, pp. 3868, 2012.
[41] T. Kuila, S. Bose, P. Khanra, A. K. Mishra, N. H. Kim, J. H. Lee. "A green approach for the reduction of graphene oxide by wild carrot root", *J Carbon.* vol. 50, pp. 914, 2012.
[42] C. Hou, Q. Zhang, Y. Li, H. Wang, J. Hazard. "P25–graphene hydrogels: Room-temperature synthesis and application for removal of methylene blue from aqueous solution", *J. Mater*. vol. 205-206, pp. 229−235, 2012.
[43] D. Luo, G. Zhang, J. Liu, X. Sun. "Evaluation criteria for reduced graphene oxide", *J. Phys. Chem*. 115, pp. 11327, 2011.
[44] K. Nakamoto. "Infrared Spectra of Inorganic and Coordination Compounds", *John Wiley & Sons: New York*, pp. 151-155, 1963.
[45] L. Tellez, F. Rubio, R. Peña-Alonso, J. Rubio. "Seguimiento por espectroscopía infrarroja (FTIR) de la copolimerización de TEOS y PDMS en presencia de TBTBol", *J. Soc. Españ. Cerám. Y Vidrio*. vol. 43, pp. 883-890, 2004.
[46] H. A. Becerril, J. Mao, Z. Liu, R. M. Stoltenberg, Z. Bao, Y. Chen. "Evaluation of solution-processed reduced graphene oxide films as transparent conductors", *ACS. J. Nano*, vol. 2, pp. 463, 2008.
[47] Y. Zhou, Q. Bao, L. Ai, L. Tang, Y. Zhong, and K. Ping Loh. "Hydrothermal dehydration for the "green" reduction of exfoliated graphene oxide to graphene and demonstration of tunable optical limiting properties", *J. Chem. Mater*., vol. 21, pp. 2950–2956, 2009
[48] H. Zhang, X. Lv, Y. Li, Y. Wang, J. Li. "P25–graphene composite as a high performance photocatalyst", *ACS J. Nano*, vol. 4, pp. 380–386, 2010.
[49] X.-Y. Zhang, H.-P. Li, X.-L. Cui, Y. Lin. "Graphene/TiO_2 composites: synthesis, characterization and application in hydrogen evolution from water photocatalytic splitting", *J. Mater. Chem.*, vol. 20, pp. 2801–2806, 2010.
[50] Y. Yao, G. Li, S. Ciston, R. M. Lueptow, K. A. Gray. "Photoreactive TiO_2/carbon nanotube composites: synthesis and reactivity", *J. Environ. Sci. Technol*., vol. 42, pp. 4952–4957, 2008.
[51] Y.-J. Xu, Y. Zhuang, X. Fu. "New insight for enhanced photocatalytic activity of TiO_2 by doping carbon nanotubes: a case study on degradation of benzene and methyl orange", *J. Phys. Chem. C*, vol. 114, pp. 2669–2676, 2010.
[52] F. Tuinstra & J. L. Koenig. "Raman spectrum of graphite", *J. of Chem. Phys.*, vol. 53, pp. 1126–1130, 1970.
[53] R. J. Nemanich, S. A. Solin. "First- and second-order Raman scattering from finite-size crystals of graphite", *J. Physical Review*, vol. 8, pp. 215, 1979.
[54] S. C. Pillai, P. Periyat, R. George, D. E. McCormack, M. K. Seery, H. Hayden, J. Colreavy, D. Corr, and S. J. Hinder. "Synthesis of High-Temperature Stable Anatase TiO_2 Photocatalyst", *J. Phys. Chem. C.*, vol. 111, pp. 1605-1611, 2007.
[55] D. Wangqi, X. Wang. "Preparation of graphite oxide (GO) and the thermal stability of silicone rubber/GO nanocomposites", *J. Thermochimica acta*, vol. 529, pp. 25-28, 2012.
[56] M. Wojtoniszaka, X. Chena, J. R. Kalenczuka, A. Wajdab, J.Łapczukb, M.Kurzewskib, M.Drozdzikb, K. P. Chuc, E. Borowiak-Palena. "Synthesis, dispersion, and cytocompatibility of graphene oxide and reduced graphene oxide", *J. Colloids and Surfaces B: Biointerfaces*. vol. 89, pp. 79-85, 2012.
[57] J. Shen, B. Yan, M. Shi, H.Ma, N. Li, M. Ye. "One step hydrothermal synthesis of TiO_2-reduced graphene oxide sheets", *J. Mater. Chem.* 21, 3415- 3421, 2011.
[58] Beyssac, B. Goffé, C. Chopin, J. N. Rouzaud. "Raman spectra of carbonaceous material in metasediments: a new geothermometer", *J. Metamorphic Geol.* vol. 20, 859–871, 2002.
[59] C. D. Wagner, W. M. Riggs, L. E. Davis, J. F. Moulder, G. E. Muilenberg. "Handbook of X-ray photoelectron spectroscopy: a reference Book of standard data for use in X-ray Photoeletron spectroscopy", *Perkin Elmer Corporation. Physical Electronics Division 6509, Flying cloud Drive, Eden Prairie, Minnesota*, pp. 55344, 1979.
[60] S. Stankovich, D. A. Dikin, R. D. Piner, K. A. Kohlhaas, A. Kleinhammes, Y. Jia, Y. Wu, S. Nguyen, R. S. Ruoff. "Synthesis of graphene-based nanosheets via chemical reduction of exfoliated graphite oxide", *J. Carbon.*, vol. 45, pp. 1558-1565, 2007.
[61] X. Li, G.Zhang, X.Bai, X.Sun, X.Wang, E. Wang, H. Dai. "Highly conducting graphene sheets and Langmuir-Blodgett films", *J. Nat. Nanotechnol.*, vol. 3, pp. 538, 2008.